

AC/DC Frequency-Dependent Power Flow Jacobian: Quantifying Grid Support and Stability Implications

Dongyeong Lee , Eros Avdiaj , and Jef Beerten 

Abstract—This letter proposes an AC/DC frequency-dependent power flow Jacobian analysis to identify the system support capabilities. In addition, the analyses reveal that system support capabilities do not necessarily enhance the system stability margin, suggesting that technical requirements of narrow-frequency-band and AC-side focused specifications may not lead to the expected performance of GFM.

Index Terms—Grid-forming, Frequency-domain Jacobian analysis, Stabilizing effect, System support, Interoperability.

I. INTRODUCTION

Power system operators and research organizations have intensified efforts to standardize the technical requirements for grid-forming (GFM) controls [1]–[4]. Among these efforts, the active and reactive power response-based transfer functions have been utilized to characterize the system support dynamics of GFM [5]. Their effectiveness for system stability analysis has been demonstrated [5], [6]. There have also been technical suggestions that utilizing this transfer function as a performance metric of GFM, focusing on the AC side with 4-40Hz [7]. In this letter, this transfer function is referred to as the frequency-dependent power flow Jacobian (FD-JB). Although these approaches provide valuable insights, they remain restricted to AC-side dynamics and to limited frequency ranges with grid-support dynamics. A lack of proper consideration of DC-side dynamics and broader frequency range of converter dynamics behavior can result in an incomplete—or even misleading—assessment of a GFM unit's ability to contribute to overall system operation and stability. In addition, the evidence is also still insufficient regarding whether the identified system supports leads to system-wide stabilization. To address these gaps, this letter proposes an analysis framework to assess system support characteristics, integration stability, and the system-stabilizing effects of GFM converters. The key contributions are summarized as follows:

- Detailed derivation of an extended AC/DC FD-JB model, representing system supportive characteristics and establishment of a formal bridging between admittance and FD-JB models.
- Proposal of a unified analysis framework for systematic evaluation of system operation support capabilities, integration stability, and system stabilizing effects with the device.
- Identification of critical limitations in technical requirements that focus primarily on AC side operation support via a limited band, which do not result in system stabilizing effects.

II. AC/DC FREQUENCY DEPENDENT POWER FLOW JACOBIAN

This section provides the derivation of the extended AC/DC FD-JB, including the bridging between admittance and FD-JB $\mathbf{J}(j\omega)$. From instantaneous AC-side active power P_{ac} , reactive Q_{ac} , and DC-side power P_{dc} of the device can be expressed based on q -axis leading and d -axis oriented dq -frame with respect to small perturbation Δ as

$$\Delta P_{ac}(s) = v_{d,0}\Delta i_d + v_{q,0}\Delta i_q + i_{d,0}\Delta v_d + i_{q,0}\Delta v_q \quad (1)$$

$$\Delta Q_{ac}(s) = v_{q,0}\Delta i_d - v_{d,0}\Delta i_q - i_{q,0}\Delta v_d + i_{d,0}\Delta v_q \quad (2)$$

$$\Delta P_{dc}(s) = v_{dc,0}\Delta i_{dc}(s) + i_{dc,0}\Delta v_{dc}(s) \quad (3)$$

where subscript 0 denotes the initial operating condition. From (1) to (3), AC/DC admittance representation can be found as

$$\Delta \mathbf{i}_{dqdc}(j\omega) = \mathbf{Y}(j\omega) \Delta \mathbf{v}_{dqdc}(j\omega) \quad (4)$$

where $\mathbf{i}_{dqdc}(j\omega) = [i_d(j\omega), i_q(j\omega), i_{dc}(j\omega)]^T$, $\mathbf{v}_{dqdc}(j\omega) = [v_d(j\omega), v_q(j\omega), v_{dc}(j\omega)]^T$ which are the components of d - and q -axis together with DC side of voltage and current. $\mathbf{Y}(j\omega)$ is AC/DC admittance. v_d, v_q are dq voltages, i_d, i_q are dq currents, and v_{dc}, i_{dc} are DC voltage and current. In this paper, all the power directions are assumed to flow out from the converter to the interconnected systems. The bold symbol denotes vectors or matrices. $|v_{ac}|, \theta_{ac}$ denote the AC-side voltage magnitude and phase angle of the device under the test (DUT). With similar manner of \mathbf{Y} , FD-JB $\mathbf{J}(j\omega)$ allows the evaluation of device dynamic characteristics at frequency ω with the power system operation aspects (P_{ac}, Q_{ac}, P_{dc} with respect to $|v_{ac}|, \theta_{ac}, v_{dc}$), which can be expressed as

$$\mathbf{J}(j\omega) = \begin{bmatrix} \underbrace{\mathbf{J}_{ac}(j\omega)}_{2 \times 2} & \underbrace{\mathbf{J}_{acdc}(j\omega)}_{2 \times 1} \\ \underbrace{\mathbf{J}_{dcac}(j\omega)}_{1 \times 2} & J_{dc}(j\omega) \end{bmatrix} \quad (5)$$

For the sake of conciseness, hereafter, (s) is omitted for brevity. To enable the deep understanding of the effectiveness and modeling method of FD-JB, \mathbf{J} should be derived. To do this, \mathbf{J} is mathematically bridged with \mathbf{Y} , while enabling efficient calculation of \mathbf{J} . To do so, the interconnecting side voltage and its phase angle, which are considered as disturbances to the device, are expressed as

$$|v_{ac}| = \sqrt{v_d^2 + v_q^2}, \quad \theta_{ac} = \tan^{-1}\left(\frac{v_q}{v_d}\right) \quad (6)$$

where $v_d = |v_{ac}| \cos \theta_{ac}$, $v_q = |v_{ac}| \sin \theta_{ac}$. $v_d = |v_{ac}|_0 + \Delta |v_{ac}|$ and $v_q = |v_{ac}|_0 \Delta \theta_{ac}$. Then, $\Delta \mathbf{v}_{dqdc}$ and $\Delta \mathbf{i}_{dqdc}$ in (1) to (3) are replaced by (4). Accordingly, \mathbf{J} can be found as

$$\begin{aligned} \Delta P_{ac} &= v_{d,0}(Y_{dd}\Delta v_d + Y_{dq}\Delta v_q + Y_{ddc}\Delta v_{dc}) + i_{d,0}\Delta v_d \\ &\quad + v_{q,0}(Y_{qd}\Delta v_d + Y_{qq}\Delta v_q + Y_{qdc}\Delta v_{dc}) + i_{q,0}\Delta v_q \\ &= \underbrace{(v_{d,0}Y_{dd} + v_{q,0}Y_{qd} + i_{d,0})}_{J_{pacv_{ac}}} \Delta |v_{ac}| \\ &\quad + \underbrace{(v_{d,0}Y_{dq} + v_{q,0}Y_{qq} + i_{q,0})}_{J_{pac\theta_{ac}}} \Delta \theta_{ac} \\ &\quad + \underbrace{(v_{d,0}Y_{ddc} + v_{q,0}Y_{qdc})}_{J_{pacv_{dc}}} \Delta v_{dc} \end{aligned} \quad (7)$$

$$\begin{aligned} \Delta Q_{ac} &= -v_{d,0}(Y_{qd}\Delta v_d + Y_{qq}\Delta v_q + Y_{qdc}\Delta v_{dc}) - i_{q,0}\Delta v_d \\ &\quad + v_{q,0}(Y_{dd}\Delta v_d + Y_{dq}\Delta v_q + Y_{ddc}\Delta v_{dc}) + i_{d,0}\Delta v_q \\ &= \underbrace{(-v_{d,0}Y_{qd} + v_{q,0}Y_{dd} - i_{q,0})}_{J_{qacv_{ac}}} \Delta |v_{ac}| \\ &\quad + \underbrace{(-v_{d,0}Y_{qq} + v_{q,0}Y_{dq} + i_{d,0})}_{J_{qac\theta_{ac}}} \Delta \theta_{ac} \\ &\quad + \underbrace{(-v_{d,0}Y_{qdc} + v_{q,0}Y_{ddc})}_{J_{qacv_{dc}}} \Delta v_{dc} \end{aligned} \quad (8)$$

This work was supported by the DIRECTIONS Project through the Energy Transition Fund, FOD Economy, Belgium.

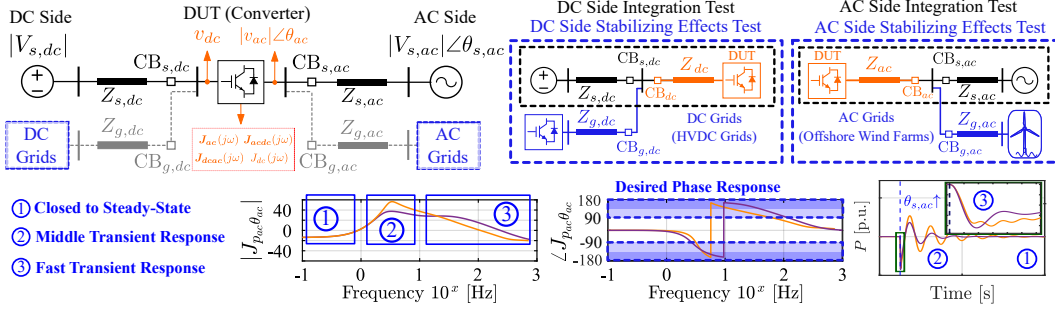


Figure 1. Unified analysis framework with a benchmark test system to test the system support capabilities, system integration stability, and stabilizing effects.

$$\begin{aligned}
 \Delta P_{dc} &= v_{dc,0} (Y_{dcd} \Delta v_d + Y_{dcq} \Delta v_q + Y_{dcdc} \Delta v_{dc}) + i_{dc,0} \Delta v_{dc} \\
 &= \underbrace{(v_{dc,0} Y_{dcd})}_{J_{pac} v_{ac}} \Delta |v_{ac}| + \underbrace{(v_{dc,0} Y_{dcq})}_{J_{pac} \theta_{ac}} \Delta \theta_{ac} \\
 &\quad + \underbrace{(v_{dc,0} Y_{dcdc} + i_{dc,0})}_{J_{pdc} v_{dc}} \Delta v_{dc}
 \end{aligned} \tag{9}$$

$$\begin{bmatrix} \Delta P_{ac} \\ \Delta Q_{ac} \\ \Delta P_{dc} \end{bmatrix} = \underbrace{\begin{bmatrix} J_{pac} v_{ac} & J_{pac} \theta_{ac} & J_{pdc} v_{dc} \\ J_{pac} v_{ac} & J_{pac} \theta_{ac} & J_{pdc} v_{dc} \\ J_{pac} v_{ac} & J_{pac} \theta_{ac} & J_{pdc} v_{dc} \end{bmatrix}}_{\mathbf{J}} \begin{bmatrix} \Delta |v_{ac}| \\ \Delta \theta_{ac} \\ \Delta v_{dc} \end{bmatrix} \tag{10}$$

As a result, \mathbf{J} quantifies the device's system support capabilities, especially with respect to the changes in $|v_{ac}|$, θ_{ac} , and v_{dc} of its interconnecting points. The bridge between \mathbf{J} and \mathbf{Y} implies \mathbf{J} also inherits the device's dynamic influences on the system stability as \mathbf{Y} does, while providing a power system-friendly interpretation.

III. UNIFIED ANALYSIS FRAMEWORK

In this section, a proposed unified analysis framework is illustrated, including how to interpret the results of \mathbf{J} and testing of the system supporting capabilities, system integration stability, and stabilizing effects. Its graphical illustration is presented in Fig. 1.

A. Benchmark Test System

The developed test system models each AC/DC side of DUT as a voltage source with its Thevenin impedance Z_s and connected to AC/DC grids through Z_g . This configuration enables a unified and flexible evaluation of system support characteristics, system-integration stability, and the stabilizing effects of the DUT by circuit breakers (CBs) and impedances. System support characteristics can be assessed by perturbing voltages, $|V_{s,ac}| \angle \theta_{s,ac}$ or $V_{s,dc}$, while $Z_s = 0$ and opening CB_g . More realistic interconnected conditions can be considered by a non-zero Z_s , which enables analysis of system integration stability with interactions between DUT and AC/DC systems. Moreover, subsystem-level studies, e.g., microgrid, can be performed by opening CB_s and closing CB_g while connecting considered sub-systems on AC/DC grids with Z_g . Finally, closing all CBs allows assessment of DUT's system stabilizing effects on the complete AC/DC system. Overall, it provides flexible frameworks that support the interoperability-oriented design of AC/DC grids.

B. Interpretation of FD-JB and Ideal Behavior in Frequency-Domain

FD-JB in the bottom part of Fig. 1 shows three sections of the frequency region with the examples of $J_{pac} \theta_{ac}$ of two cases (purple and orange colors) and time-domain response results when it is tested

via $Z_s = 0$ and all CB_g opened. The low-frequency band represents the very slow response, which is close to steady-state. The middle frequency band represents a relatively slow transient response, while the high frequency band represents a relatively fast transient response. These middle and high frequency bands can present expected GFM's system operational supports (e.g., 4-40Hz in [7]). For the magnitude, a higher value denotes a stronger response from the DUT. The phase information of \mathbf{J} is also important to have desired supporting characteristics as it is related to the response direction with respect to the system changes, particularly, considering $J_{pac} \theta_{ac}$, $J_{qac} v_{ac}$, and $J_{pdc} v_{dc}$ to support power system operation. Therefore, the desired GFM's dynamic responses for system operation support are a larger magnitude and a phase angle closer to 180° , which reflect a better response of GFM by resisting the changes of the system. In the example of $J_{pac} \theta_{ac}$ in Fig. 1, the purple line shows a higher magnitude in the high frequency band, a lower magnitude in the middle frequency, and the same one in the low frequency compared to the orange line. Time-domain responses show alignment with $J_{pac} \theta_{ac}$. According to $J_{pac} \theta_{ac}$, the purple line shows a stronger response in the initial transient but a weaker late transient, eventually showing a similar tendency compared to the orange line as they get closer to the steady state. However, even though it demonstrates its effectiveness in validating the system operation support aspect, further investigation is required to verify its implications for system stability.

IV. CASE STUDIES

In this section, case studies are presented to investigate the implications of FD-JB on the system stability. The used DUT considers a modular multilevel converter and control schemes are virtual synchronous machine for GFM with virtual inductance L_v , grid-following (GFL) with DC voltage droop between v_{dc} and p_{ac} as $e_p = K_{d,dc}(v_{dc} - v_{dc}^*) + p_{ac}^* - p_{ac}$. e and superscript $*$ denote the error and reference signals for control loops with droop gain $K_{d,dc}$.

A. System Support Capabilities & Integration Stability

Using the developed test system, system-supportive characteristics are tested to verify the effectiveness of the proposed extended AC/DC \mathbf{J} by opening all CB_g . Corresponding \mathbf{J} is presented focusing on $J_{pac} \theta_{ac}$, $J_{qac} v_{ac}$, and $J_{pdc} v_{dc}$ in Fig. 2. Here, $P \& Q$ case refers to the case of GFL with $K_{d,dc} = 0$. $P_{ac,0} = 1.0$ p.u. is assumed.

For the time-domain test of 0-3s, $\Delta \theta_{s,ac} = 2^\circ$, $\Delta |V_{s,ac}| = 0.01$ p.u., $\Delta V_{s,dc} = 0.01$ p.u. are sequentially applied and restored at 3.5s. It shows aligned response results corresponding to \mathbf{J} . While GFM shows a meaningful response to AC side disturbances at 0.5s and 1.5s, it draws a significant ΔP_{dc} . Therefore, without proper consideration of DC-side dynamics, the expectations of system support from GFM might differ from the results of AC-side-only considerations. GFLs with $K_{d,dc}$ show a significant $\Delta P_{dc} \& \Delta P_{ac}$,

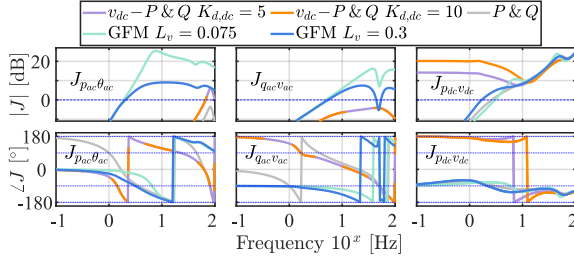


Figure 2. FD-JB of $J_{pac\theta_{ac}}$, $J_{qacv_{ac}}$, and $J_{pdcv_{dc}}$ with different converters.

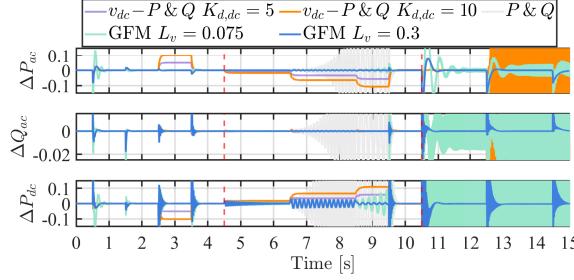


Figure 3. EMT results of system support and weak grid integration tests.

including a steady-state response according to droop control, i.e., due to the increases in v_{dc} . It confirms the effectiveness of \mathbf{J} in system operational supporting characteristics. For 4.5-9.5s, DC weak grid stability is tested with sequential increases of $Z_{s,dc} = [0.001 + j0.15, 0.0035 + j0.525, 0.006 + j0.9]$ in p.u. and restored at 9.5s. GFLs without droop cannot be stable; however, GFLs with $K_{d,dc}$ remain stable even as the system weakens. Notably, GFM with a lower L_v shows instability while the other does not. After 10.5s, AC weak grid stability is tested with sequential increases of $Z_{s,ac} = [j0.325, j0.425, j0.475]$ in p.u. As a result, only the GFM with a higher L_v shows stable results, while the other GFM and GFLs do not. It shows that even though $L_v = 0.075$ has a stronger supporting feature on the AC side, it does not confer standalone stability. Therefore, better system support capabilities can not guarantee better stability. The results demonstrate the effectiveness of the test system for evaluating system operation support and system integration stability. However, the implication of \mathbf{J} on overall system stabilization remains unclear. For this aspect, AC/DC sides are individually tested, considering the subsystem with GFL $P\&Q$ in later subsections, by closing CB_g with $|Z_g| = 0.01$ p.u. For each side of the test, the other is with an ideal voltage source.

B. Stabilizing Effects Analysis with DC Weak Grid

The DC side stabilizing effects test results are shown in Fig. 4. $Z_{s,dc} = [0.0018 + j0.27, 0.0024 + j0.36]$ in p.u. are sequentially applied at 1s and 6s. The results show that even though the $K_{d,dc} = 5$ case is stable when it is considered with a weak grid integration without subsystem consideration in Fig. 3, it fails to stabilize the system. Meanwhile, $K_{d,dc} = 10$ shows stable results with the subsystem. It implies that a superior \mathbf{J} might lead to better stabilizing effects as long as its own stability is guaranteed.

C. Stabilizing Effects Analysis with AC Weak Grid

The AC side stabilizing effects test results are shown in Fig. 5. $Z_{s,ac} = [j0.22, j0.245]$ in p.u. are sequentially applied at 1s and 6s. As the low-frequency band of $J_{pac\theta_{ac}}$ and $J_{qacv_{ac}}$ in Fig. 2 are small and similar, GFLs do not show meaningful differences while getting

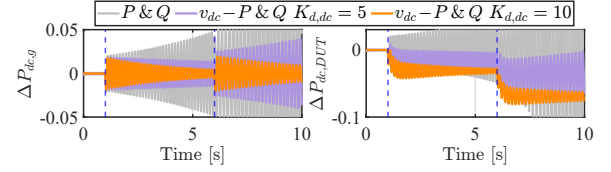


Figure 4. EMT results of DC side stabilizing effects where DC weak grid with $|Z_{s,dc}|$ increases at 1s and 6s.

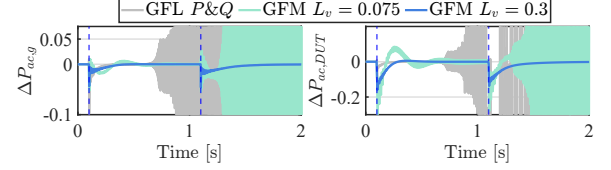


Figure 5. EMT results of AC side stabilizing effects where AC weak grid with $|Z_{s,ac}|$ increases at 1s and 6s.

closer to steady-state. For the middle and high-frequency bands of FD-JB, the lower L_v case shows a higher magnitude. Therefore, a lower L_v is expected to yield better support characteristics. Indeed, it shows a better instantaneous system-supportive response, which aligns with [7]. This can be seen between 0.1s and 1.1s. At 1.1s, even though with better system support characteristics, a lower L_v case gets unstable as the system weakens. If only examining FD-JB, a lower L_v case is expected to bring better stabilizing effects as in section IV-B. However, it shows that system support does not result in stabilizing effects because its own system stability is not guaranteed under the weak grid condition, as observed in Fig. 3. As a result, better system support does not necessarily bring better stabilizing effects. Therefore, it is not enough to consider only system support characteristics (4-40Hz) from FD-JB to fulfil the expectations of GFM, such as improving the system stability.

V. CONCLUSIONS

In this letter, AC/DC FD-JB is proposed and demonstrated its effectiveness through the developed test system. In addition, analysis results reveal that AC side and limited band focusing evaluation of GFM may lead to misleading expectations, e.g., system support capabilities do not necessarily imply better system stability contribution. Instead, whether it fulfills the GFM's expectations also depends on its stability with the system condition. Therefore, while AC/DC FD-JB provides meaningful guidance on system support characteristics, holistic assessment of overall system stability remains essential for the reliable design of interoperable AC/DC grids.

REFERENCES

- [1] ESO, "Great britain grid forming best practice guide," 2023.
- [2] AEMO, "Voluntary specification for grid-forming inverters: Core requirements test framework," 2024.
- [3] NERC, "Grid forming functional specifications for bps-connected battery energy systems," 2023.
- [4] ENTSO-E, "Grid forming capability of power park modules: Report on technical requirements," 2025.
- [5] S. Shah, W. Yan, P. Koralewicz, V. Gevorgian, D. Ramasubramanian, R. Wallen, A. Hoke, B. Kroposki, and B. Mather, "A testing framework for grid-forming resources," in *2023 IEEE Power & Energy Society General Meeting (PESGM)*, 2023, pp. 1–5.
- [6] K. Dey and A. M. Kulkarni, "Passivity-based decentralized criteria for small-signal stability of power systems with converter-interfaced generation," *IEEE Transactions on Power Systems*, vol. 38, no. 3, pp. 2820–2833, 2023.
- [7] ESIG, "Testing the performance of grid-forming resources: Test methods and performance metrics for evaluating the voltage source behavior of grid-forming resources," 2025.